Article:
Johnson, R.C., Royapoor, M. and Mayfield, M. orcid.org/0000-0002-9174-1773 (2021) A multi-zone, fast solving, rapidly reconfigurable building and electrified heating system model for generation of control dependent heat pump power demand profiles. Applied Energy, 304. 117663. ISSN 0306-2619

https://doi.org/10.1016/j.apenergy.2021.117663

Applied Energy 304 (2021) 117663

Contents lists available at ScienceDirect

Applied Energy

journal homepage: www.elsevier.com/locate/apenergy

A multi-zone, fast solving, rapidly reconfigurable building and electrified heating system model for generation of control dependent heat pump power demand profiles

R.C. Johnson [a,*], M. Royapoor [b], M. Mayfield [a]

[a] Department of Civil and Structural Engineering, University of Sheffield, UK
[b] School of Engineering, Newcastle University, UK

HIGHLIGHTS

- A dynamic, multi-zone model for heat pump demand profile simulation is presented.
- The model is capable of rapid simulation at 5 s resolution.
- The model is suited to batch simulation of multiple building profiles.
- An interface that allows control logic modification is provided.
- Results are consistent when compared to real data and equivalent EnergyPlus models.

ARTICLE INFO

Keywords:
Building simulation
Heat pumps
Electrified heating
Heating system control

ABSTRACT

The electrification of heating is expected to grow in the UK domestic sector, and this has increased interest in the effects that this may have on low and high voltage network operation. However, Electrified heating profiles that alter with control decisions can only be obtained from dedicated building modelling that energy system modellers do not usually have the expertise to perform, yet these are required for meaningful studies. This work outlines a novel method for modelling air source and ground source heat pump power demand profiles using a multi-zone physics based building modelling framework with building fabric, thermohydraulic, and air flow subsystems. The novel setup framework allows detailed building layout, fabric and control properties to be assigned by analysts with no prior building modelling expertise. Once fully assigned, the building model can be used to generate heat pump power demand profiles at sub minute resolution. Upon testing, a single daily run of the model could be executed in 17 s. The model was then validated against real life test house data, under various control and weather conditions. A small relative error (typically within 10%) was observed between modelled and actual cycle lengths, and modelled and actual heat and electricity demands. Due to its rapid solution rate, the model is of significant value to energy efficiency and distribution network studies, where large demand profile sets that are sensitive to detailed retrofit and control considerations are often essential. The model has been made openly available.

1. Introduction

The IPCC 1.5 °C report notes that adverse impacts on human and natural systems are already being observed as a result of global warming, and emphasises the need to adapt behaviours in order prevent a global temperature rise of 2 °C above pre-industrial levels [1]. Decarbonisation pathways often outline the importance of decarbonisation of electrical power systems, in part because this would allow low carbon electrification of heating. It is therefore important to consider the operational and behavioural changes that may arise from building heating loads being transferred onto electrical grids.

Falling systems costs [2] and the availability of the renewable heat incentive (RHI) [3] tariff are beginning to make installation of electrified heating technologies economically attractive to the homeowner. However, unless adequately managed, the resulting peak electrical demand increase is expected to heavily impact the operation of distribution and transmission networks [4]. This has led the research community to

* Corresponding author.

https://doi.org/10.1016/j.apenergy.2021.117663
Received 25 May 2021; Received in revised form 10 August 2021; Accepted 18 August 2021
Available online 6 September 2021

Nomenclature

Common variables

A	Area (m^2)
ACR	Air changeover rate ($hour^{-1}$)
α	Heat transfer coefficient (non-conductive) (W/m^2 k)
c	Specific heat capacity (kg/m^3)
C_D	Discharge coefficient (dimensionless)
E	Energy (J)
ELA	Equivalent leakage area (cm^2/m^2, or cm^2/m dependent on use case)
g	Gravitational constant (9.81 m/s^2)
H	Total doorway height (m)
h	Height of evaluation (m)
Δh	Height of doorway interval (m)
I	Irradiance (W/m^2)
L	Duration (s)
m	Mass (kg)
$\dot{m}$	Mass flow rate (kg/s)
N	Total number of object defined in subscript (dimensionless)
P	Power output/Input (W)
$\dot{Q}$	Heat flow rate (W/s)
R	R-Value (m^2 k /W)
ρ	Density (kg/m^3)
T	Temperature (K)
ΔT	Temperature difference between (K)
θ	Irradiance angle (radians)
U	U-Value (W m^{-2} k^{-1})
V	Volume (m^3)
v	Velocity (m/s)
W	Width (m)
X	Binary variable denoting whether a system is on (1) or off (0) (dimensionless)

Common subscripts

air	Of 1 kg of air at standard temperature and pressure
avg	Average
bypass	Through the bypass valve
cond	Relating to conductive heat transfer
conv	Relating to convective heat transfer
DHWTank	Of/through the DHW tank
diffH	Of the diffuse horizontal component
DNI	Of the direct normal component
e	Electrical
ext	Of/on/through external node of outer wall
g	Of the ground below the foundations
hcond	Of the air in the room linked conductively (via a separating wall) to the current room
H_2O	Of 1 kg of water at 298 K
in→out	Difference between inside and outside (typically used for temperature and pressure)
Inf/Ven	Resulting from infiltration and ventilation air flows
int	Of/on/through internal node of outer wall
intermed	Relating to the floor/ceiling separation between a room and the room directly above/below it
LW	Relating to long-wave radiative transfer
mid	Of/on/through midpoint node of outer wall, usually represents a cavity or filled cavity
nom	Under nominal operating conditions
on	'On' component of heat pump cycle
out	Of outdoors (usually temperature or pressure)
rad	Of/from the water contained in a radiator (or radiative form of heat transfer where implied)
ref	Reference value
rf	Of/through roof Insulation
room	Of the air contained within the room
set	Set point
sl	Of/through/to the concrete slab
step	Relating to step size (used only for time)
stf	Of/through the suspended timber floor
SW	Relating to short-wave solar gain on an outer wall
th	Thermal
total	Entire heat pump cycle (both on and off sections)

investigate building heating management and fabric retrofit strategies that can relieve electrical grid congestion. For example, Navarro Espinosa et al. examined the effects of building retrofit and network reinforcement on the magnitude of thermal and voltage violations on distribution networks [5], Pimm et al. further expanded on this to examine the effects of including electrical energy storage (though did not included detail network analysis [6]. Johnson et al developed upon these studies by examining the impacts of electrical energy storage, heat pump type (ASHP or GSHP), and heat emitter type (radiator or underfloor) on grid congestion [7]. However, none were able to consider changes in multi-zone or detailed system parameters such as thermostatic radiator valve (TRV) setting changes, zone thermostat control, pump control strategies, DHW tank operational changes, and combined vehicle and air source heat pump (ASHP) or ground source heat pump (GSHP) management. Better understanding of building scale electrified heating control and retrofit and its impact on power systems remains a priority, particularly as electrified heating technologies gain greater share of the market.

Commercially available building simulation packages such as EnergyPlus (E+) [8], and readily available models with heating demand capabilities such as the Centre for Renewable Energy Systems Technology (CREST) model do not allow dynamic control to be simulated at the temporal and spatial resolutions required to analyse all forms of controls [9]. For example, minute or sub minute output profiles may be desirable when performing network constraint studies, and control systems with many components must often be simulated at sub minute resolution to ensure simulation stability. Whilst it is possible to produce models that emulate some degree of control in packages such as E+ or TRNSYS, these platforms require detailed expertise that most practising engineers lack. Additionally, creating high fidelity models using these systems can be extremely time-consuming and most of the simulation output from these packages are not required by an analyst whose focus is electricity and heat demand profiles.

Fast full building models have been developed, but these are not suited to bulk scale multi-zone modelling of UK stock. Laughman et al. developed a multi-zone electro-thermal model of a US domestic residence [10], with convective, radiant and ventilation subsystem models. However, this is not suitable for modelling of typical UK hydronic heating systems, and does not consider room level zoning (each zone represents one floor). A similar model able to consider living and non-living areas as separate zones, each with hydronic heating via ASHP systems - was presented by Hong et al. [11]. The model was able to assess the electro-thermal load shifting capability of 2 different UK residences with heat pump and buffer tanks under different control schemes, but is unsuited to rapid parametrization, and does not include room level zoning. Similar work was presented by Perera et al., though this model did not consider hydronic heating. Other multi-zone models, such as Shoeboxer, are suited to district scale modelling, specific,

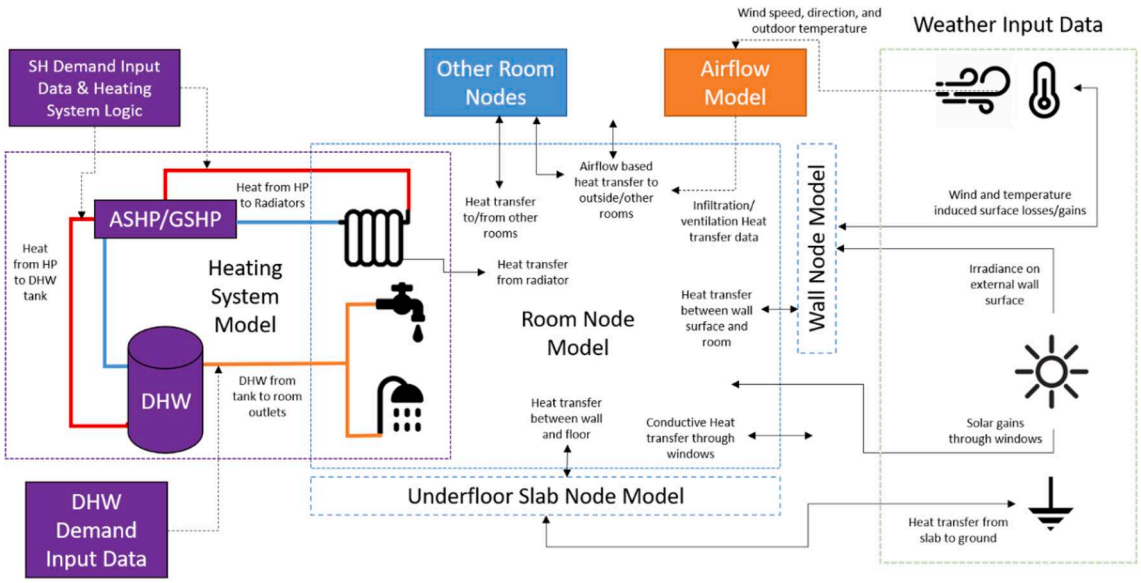

Fig 1. The overall structure of the model and interactions between sub-models and datasets.

customisable control and interractions [12]. Computationally efficient components of full building models have been explored in research. Wetter presented a single room node model for development of a modelica multi-zone model. However, this does not address the issue of rapid full building parameterization, and did not consider sizing of radiative and convective heating sources [13].

Alternatively computational fluid dynamics (CFD) based packages are available that allow for control strategies to be programmed accurately, but these typically are complex to initialise, need extremely fine temporal and special resolutions and may fail to converge on a solution [14]. Researchers have recently explored fast fluid dynamics (FFD) as a solution to slow CFD models, and have achieved simulations rates of up to 3.5 times real time [15]. Whilst this is the state of the art for applications where detailed heat and air flow information is required, such tools are too slow for generation of daily ASHP/GSHP demand profiles, and also too complex for the general energy analyst.

Therefore a gap exists for a readily executable tool that can [i] allow estimation of high resolution heat pump demand profiles (including defrost) for multi-zoned residential buildings [ii] enable quick creation of a multi-zone residential building geometry and its control settings without having to extensively parameterise building fabric and components [iii] allow batch simulation (hundreds - thousands of runs) of ASHP/GSHP demand profiles at an acceptable rate [iv] enable performance and load profile characterisation of any heat pump (HP) type or size with duty cycles varying realistically as a function of weather and system control, while capturing the full impacts of building fabric thermo-physical properties, occupant interactions, and weather variations. This work seeks to address this gap by introducing a first-principle based tool referred to as Electrified Water and Space-heating Profiler (EWASP) model that offers the following advantages:

- Accurate generation of ASHP and GSHP heat and electricity profiles at high temporal resolution, at a rate fast enough for multiple building studies, allowing for space heating and DHW segregation.
- Modifiable pre-programmed building archetypes that represent typical UK domestic properties, so that the model can be readily accessible to researchers with no prior building physics knowledge, and those who require quick simulation of many residential buildings with different fabric and layout properties.
- Means to modify heating system and building properties at a room level of spatial granularity, with no need for building modelling expertise.
- An interface to allow quick modification of the control system (e.g. for Demand Side Management, battery charging, etc.)

The model is therefore suited to studies into both the effects of control and retrofit on building energy efficiency, and the effects these operational changes may have on multi-building systems, such as low voltage power networks.

The governing equations that underpin EWASP are outlined in the method section. A two stage model validation is then undertaken by [i] comparing the model results to real test data collected from an actual building and [ii] offering comparative results of both computational time and prediction accuracy between the EWASP model and an identical building model using E+. The latter validations are performed across multiple days to demonstrate the much faster, yet still accurate simulation capabilities of EWASP.

2. Methodology

The following section outlines the modelling methodology used to develop a nominal domestic building model and its associated heating system.

2.1. Modelling overview

In order to simulate a multi-zone residential building, the following interacting sub-models (or components) are required:

i. Room and building node sub-model: this determines radiative and conductive heat transfer across building fabric elements, as a function of room air temperature, and envelope surface temperatures.
ii. Airflow network sub-model: this calculates convective heat transfer throughout the building (i.e. ventilation and infiltration) as a function of internal to outdoor temperature differences, wind speed, wind direction, and the overall layout of the building. This component interacts with the room node component by providing a value for overall convective heat gain/loss per second as a result of infiltration
iii. Heating system sub-model: This component models the behavior of the heating system, as a function of system control logic settings and heat pump description, and interacts with the room node component via heat transfer from radiators to rooms.

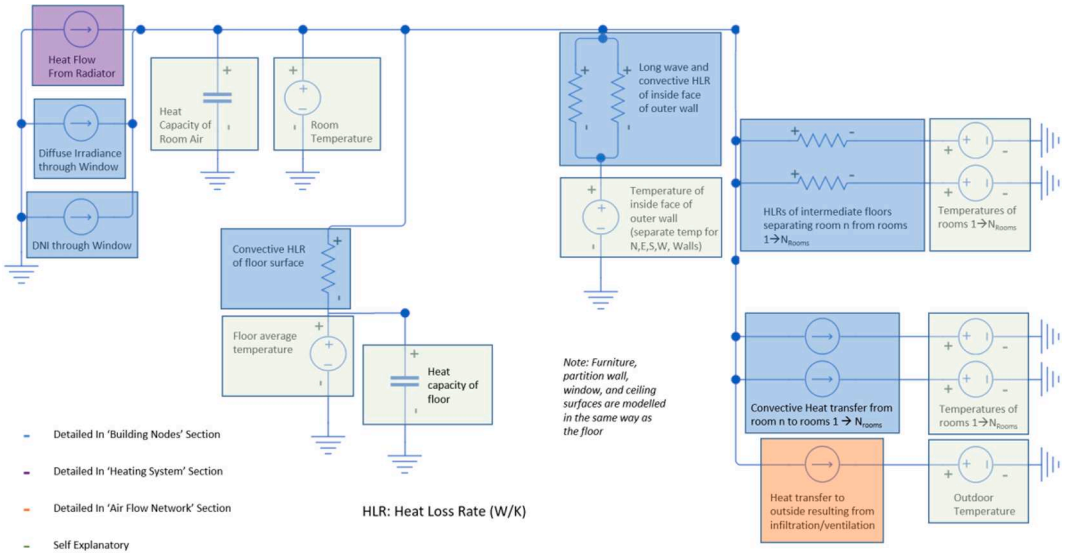

Fig. 2. Electrical circuit analogy describing the 'Room node sub-model' of a single zone.

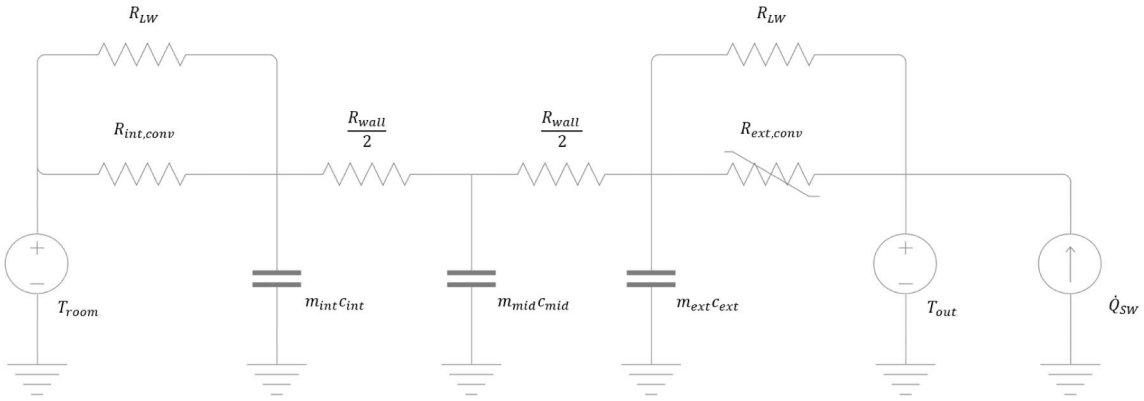

Fig. 3. Equivalent circuit representation of the room node R_{LW}, R_{conv}, and R_{wall} involving the long wave (infrared) radiative, surface convective, and conductive resistances to heat flow.

The overall model also requires various sets of input weather and demand data, and a control logic script. Fig. 1 illustrates how the overall model and its constituent components interact.

2.2. Room and building node sub-models

Conductive and radiative gains or losses for any given room are determined using the room node sub-model, and its associated building node components which represent outer walls and floors. Fig. 2 summarises the room node component using electrical circuit analogy.

The temperature change of the air within any room node is modelled using Eq. (1):

$$\frac{\partial T_{room}}{\partial t} = \frac{1}{m_{air}c_{air}}\left[-\dot{Q}_{\frac{Inf}{Ven}} - \dot{Q}_{fl} - \dot{Q}_{rf} - \dot{Q}_{wall} - \dot{Q}_{win} - \dot{Q}_{intermed} - \dot{Q}_{sep} - \dot{Q}_{furniture} + \dot{Q}_{rad}\right] \quad (1)$$

where $\dot{Q}_{Inf/Ven}$ represents combined ventilation and infiltration heat loss and is calculated separately for each room using the airflow sub-model (see Section 2.4). $\dot{Q}_{wall}$ represents heat transfer to the internal faces of outer walls via long wave radiation and convective air motion within the room as in Eq. (2):

$$\dot{Q}_{wall} = \sum_{n=1}^{4}\left[\alpha_c\left(T_{room} - T_{int,n}\right) + \alpha_{LW}\left(T_{room} - T_{int,n}\right)\right]A_{wall,n} \quad (2)$$

α_c and α_{LW} are convective and long-wave radiative heat transfer coefficients, and take values of 2.5 W/m^2•K and 5.6W/m^2•K (see [16] for justification). The index numbers $n = 1:4$ represent the north, east, south, and west walls respectively. For clarity, if a zone has no east or west outdoor wall (which would almost always be the case for a south facing mid-terraced house), $A_{wall,2}$ and $A_{wall,4}$ are set to zero.

A wall model must be coupled with equations 3a-3c to allow $T_{int,n}$, to change with heat transfer. Any outer wall is represented by 3 nodes (interior, middle, and exterior) using a typical Beuken model [17], as follows:

$$\begin{bmatrix} \frac{\partial T_{int}}{\partial t} \\ \frac{\partial T_{mid}}{\partial t} \\ \frac{\partial T_{ext}}{\partial t} \end{bmatrix} = \begin{bmatrix} -\frac{2U_{wall}}{c_{int}m_{int}} & \frac{2U_{wall}}{c_{int}m_{int}} & 0 \\ \frac{2U_{wall}}{c_{mid}m_{mid}} & \frac{-4U_{wall}}{c_{mid}m_{mid}} & \frac{2U_{wall}}{c_{mid}m_{mid}} \\ 0 & \frac{2U_{wall}}{c_{ext}m_{ext}} & -\frac{2U_{wall}}{c_{ext}m_{ext}} \end{bmatrix} \begin{bmatrix} T_{int} \\ T_{mid} \\ T_{ext} \end{bmatrix} + \begin{bmatrix} \frac{1}{c_{int}m_{int}} & 0 & 0 \\ 0 & \frac{1}{c_{mid}m_{mid}} & 0 \\ 0 & 0 & \frac{1}{c_{ext}m_{ext}} \end{bmatrix} \begin{bmatrix} \zeta_1 \\ \zeta_2 \\ \zeta_3 \end{bmatrix} \tag{3a}$$

$$\begin{bmatrix} \zeta_1 \\ \zeta_2 \\ \zeta_3 \end{bmatrix} = \begin{bmatrix} [\alpha_{conv}(T_{room} - T_{int}) + \alpha_{LW}(T_{room} - T_{int})]A_{wall} \\ 0 \\ \left[(2.8 + 3v_{wind} + \alpha_{LW})(T_{room} - T_{ext}) + \dot{Q}_{SW}\right]A_{wall} \end{bmatrix} \tag{3b}$$

where U_{wall} is the conductive heat transfer in W/m^{2}K for the entire thickness of the outer wall, $c_{int}, c_{mid}, c_{ext}$ and $m_{int}, m_{mid}, m_{ext}$ are the specific heat capacities and total mass of the internal, mid, and external nodes. α_{conv} represents conductive heat transfer from the zone air to the internal node of the outer wall, and has units W/m^{2}K. v_{wind} is wind speed (used to modify heat transfer to the environment on the external face of the outer wall), and $\dot{Q}_{SW}$ is the solar gain on the wall surface, which is calculated using Eq. (3c) [18],

$$\dot{Q}_{SW} = cos(\theta_{DNI,ext})A_{ext}I_{DNI,ext} + \frac{A_{ext}I_{diffH,ext}}{2} \tag{3c}$$

where $\theta_{DNI,ext}$ is the angle between the incident direct irradiance and the normal to the wall surface, and $I_{diffH,ext}$ is horizontal diffuse irradiance.

Each face of a rooms outer wall is modelled as a separate node, because short wave (solar) irradiance on the surfaces vary with the relative angle between the wall and the sun. Room node principles are summarised in Fig. 3 using electrical circuit analogy.

This methodology (and the Beuken methdolgy used for all following fabric elements) is similar to that used in more detailed modelling platforms, such as E+, though involves fewer nodes.

Equations 4a-4d outline the treatment of floor thermal dynamics in which heat flow via floors ($\dot{Q}_{sl}$) is calculated using Eq. (4a):

$$\dot{Q}_{sl} = A_{fl}\alpha_{conv,fl}\left(T_{room} - T_{int,fl}\right) \tag{4a}$$

And temperatures of the internal, mid and external floor nodes ($T_{int,fl}$, $T_{mid,fl}$, $T_{ext,fl}$) are updated using:

$$\begin{bmatrix} \frac{\partial T_{int,fl}}{\partial t} \\ \frac{\partial T_{mid,fl}}{\partial t} \\ \frac{\partial T_{ext,fl}}{\partial t} \end{bmatrix} = \begin{bmatrix} -\frac{2U_{fl}}{c_{int,fl}m_{int,fl}} & \frac{2U_{fl}}{c_{int,fl}m_{int,fl}} & 0 \\ \frac{2U_{fl}}{c_{int,fl}m_{int,fl}} & \frac{-4U_{fl}}{c_{int,fl}m_{int,fl}} & \frac{2U_{fl}}{c_{int,fl}m_{int,fl}} \\ 0 & \frac{2U_{fl}}{c_{int,fl}m_{int,fl}} & -\frac{2U_{fl}}{c_{int,fl}m_{int,fl}} \end{bmatrix} \begin{bmatrix} T_{int,fl} \\ T_{mid,fl} \\ T_{ext,fl} \end{bmatrix} + \begin{bmatrix} \zeta_1 \\ \zeta_2 \\ \zeta_3 \end{bmatrix} \tag{4b}$$

$$\begin{bmatrix} \zeta_1 \\ \zeta_2 \\ \zeta_3 \end{bmatrix} = \begin{bmatrix} \frac{\left[\left(\alpha_{conv,fl} + \alpha_{LW}\right)\left(T_{room} - T_{int,fl}\right)\right]A_{fl}}{c_{int,fl}m_{int,fl}} \\ 0 \\ \frac{A_{fl}\left(2U_{fl}\right)\left(T_{ext,fl} - T_g\right)}{c_{int,fl}m_{int,fl}} \end{bmatrix} \tag{4c}$$

where U_{fl} represents is the conductive heat transfer in W/m^{2}K for the entire thickness of the floor, A_{sl} is the total floor area of the room, $T_{int,fl}$, $T_{mid,fl}$, $T_{ext,fl}$, are the internal mid, and external floor node temperatures, and the constant $\alpha_{conv,fl}$ is the convective heat transfer rate between the room and the floor surface (fixed to 2.0 W/m^{2}K, as suggested by [16]).

Long wave radiative transfer (α_{LW}) is modelled using the same constant as is used for the wall surfaces. Floor nodes are included for solid concrete flooring only. For suspended timber floor, Eq. (4a) becomes:

$$\dot{Q}_{stf} = A_{stf}U_{stf}(T_{room} - T_{out}) \tag{4d}$$

Where $\dot{Q}_{stf}$ represents the conductive heat loss from the room via conductive transfer through a suspended timber floor.

Conductive loss through ceiling and roof ($\dot{Q}_{rf}$) is modelled using a similar Beuken model [19]. However, the internal node represents the top floor ceiling mass (plaster, timber etc.), the mid node represents the loft space, and the outer node represents the mass of the roof (slates/tiles, battens, barriers etc.), which can absorb solar irradiance. Furthermore, whilst all top floor rooms have a separate internal ceiling node, they share the same mid and external roof nodes.

Heat lost through windows ($\dot{Q}_{win}$) are modelled to include an internal and external node (double glazing as two separate panes and single glazing as two half panes) [16]. The convective heat transfers between separate double glazing panes (or conductive transfer between halves of single glazing panes) are based on representative U values. Both window nodes can absorb solar energy, and the absorption rate is a function of irradiance and incidence angle (see [18] for an explanation of effective irradiance incidence angle, and [20] for details on window modelling)

$\dot{Q}_{wall,sep}$ is convective heat loss to internal wall surfaces, and is calculated as the sum of the loss though all separating boundaries (Eq. (5)).

$$\dot{Q}_{wall,sep} = \sum_{n=1}^{N_{hcond}} A_{wall,sep,n}\alpha_{conv}\left(T_{room} - T_{wall,sep,n}\right) \tag{5a}$$

The summation operator allows the user to consider the wall area on each face of the room separately – where compass directions N, E, S, & W are referred to by n = 1, 2, 3 & 4 respectively. $T_{wall,sep,n}$ is the temperature of the internal wall surface associated with compass direction n.

Each internal wall is modelled as an external wall with the exeption that the nodes represent the 2 wall surfaces on either side of the partition, and the cavity between these two surfaces.

$\dot{Q}_{intermed}$ represents the vertical analogue of $\dot{Q}_{wall,sep}$ i.e. conductive heat transfer between the room node and rooms that lay directly above/below it.

Conductive heat transfer between each room node and rooms directly above/below ($\dot{Q}_{intermed}$) are represented by Eq. (5b). $\dot{Q}_{intermed}$is able to account for the area of overlap ($A_{intermed,int}$) between rooms sharing a common intermediate floor, and the number of overlapping rooms (N_{vcond}):

$$\dot{Q}_{intermed} = \sum_{n=1}^{N_{vcond}} A_{intermed,n}U_{intermed}\left(T_{room} - T_{vcond,n}\right) \tag{5b}$$

where $A_{intermed,n}$ is the area of overlap between the room and its cross-intermediate floor neighbor 'n', $T_{vcond,n}$ is the temperature difference between the rooms and $U_{intermed}$ is the intermediate floor U-value. The intermediate floor U-value considers typical thermal properties of floorboards [21], underlay [22], and carpets [23].

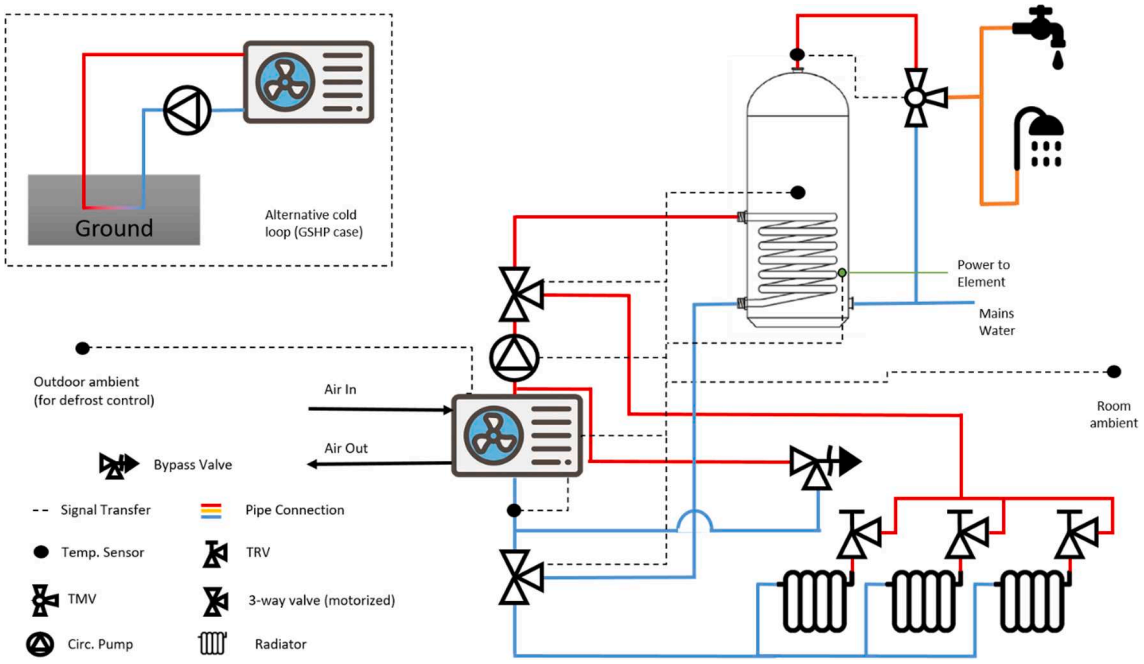

Fig 4. Heating system schematic and associated control links.

Table 1
Heating system control logic. The columns with the heading 'Hyst. Cross' describe the hysteresis limit that the temperature last crossed e.g. the value 'Low' means temperature fell below the lower limit of the band more recently than it rose above the upper limit.

Defrost Required?	Tank Temp. Hyst. Cross	Tank Return Hyst. Cross	10 min Limiter Satisfied	Room Thermo. Cross	SH Return Hyst. Cross	Heat Pump	SH Circ.	DHWCirc.
Yes	Low	N/A	Any	Any	N/A	Defrost	Off	On
Yes	High	N/A	Any	Any	N/A	Defrost	On	Off
No	Low	Low	Any	Any	N/A	On	Off	On
No	Low	High	Any	Any	N/A	Off	Off	On
No	High	N/A	No	Any	Any	Off	Off	Off
No	High	N/A	Yes	Low	Low	On	On	Off
No	High	N/A	Yes	Low	High	Off	On	Off
No	High	N/A	Yes	High	High	Off	Off	Off

Table 2
Control logic for the auxiliary top up DHW direct heater.

Upper Thresh. < Tank Temp. < 60	All other control variables	Aux Heater
Yes	Any	On
No	Any	Off

$\dot{Q}_{furniture}$ represents the heat exchange with the soft, wooden, and plastic furnishings within a zone. Furniture is modelled using the virtual sphere method [24], which allows bulk modelling of each furniture type as a single node with a surface temperature, average temperature, heat capacity, and effective surface area. Typical masses and surface areas of each furniture type per unit floor area are obtained from [25].

$\dot{Q}_{rad}$ represents the heat gain from the room radiator. $\dot{Q}_{rad}$, and radiator node temperatures are all calculated using the '210' 2-node model [26]. The model is valid in all flow rate situations (up to a timestep of 60 sec), and so is appropriate for use where TRV control is employed.

$\dot{Q}_{solar}$ approximates solar gains through windows as a dynamic function of horizontal diffuse irradiance, direct normal irradiance, and irradiance incidence angles,

$$\dot{Q}_{solar} = \sum_{n=1}^{4} TF\left(\theta_{DNI,n}\right) A_{win,n} I_{DNI,n} + TF\left(DIFF\left(\theta_{eff,d}\right)\right) \frac{A_{win,n} I_{diffH,n}}{2} \quad (6)$$

In which $DIFF\left(\theta_{eff,d}\right)$ computes an effective diffuse angle for irradiance on a transparent surface derived from [18], then the transmission function TF approximates the fraction of the incident diffuse irradiance transmitted through the window, based on empirical observations [20]. The ½ factor arises from the fact that the window is at a 90° tilt, and therefore is exposed to only half of the total diffuse irradiance (i.e. isotropic distribution of diffuse irradiance is assumed). The TF function is also applied to direct irradiance, and both components are adjusted for irradiance (direct normal and diffuse horizontal respectively) and total window area. The summation operator allows the model to consider the window area on each face of the room separately. To clarify, if the room has windows on the north and south faces, the solar gains will be computed separately for each face, then the 2 results will be summed. If no windows exist on a given face, $A_{win,n}$ is set to 0. This term doesn't appear directly in Eq. [1] since irradiance gains are not applied directly to the room, but split equally across internal surfaces.

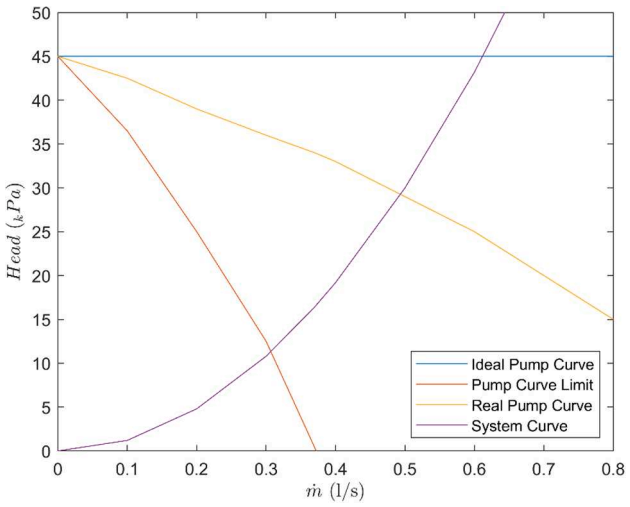

Fig. 5. A comparison of pressure vs. flow between a pump that produces constant pressure (Ideal Pump Curve) and a real circulation pump curve (Real Pump Curve) and finally the pressure- flow response that would be required to invalidate the constant pressure approximation (pump curve limit). System Curve illustrates the pressure-flow behavior used in test house model in this study (baseline data reproduced from [27]).

2.3. Heating system model

2.3.1. Overview of the heating system model

The overall heating system topology is summarized in Fig. 4. The system consists of an ASHP or GSHP, that serves a DHW tank and also a series of radiators of definable capacity, either preset as a default or entered by the analyst. If a GSHP is chosen, underground heat exchange tubing is also modelled. HP bypass valves, 3 way mixing valves, and TRVs are modelled to better represent a typical real-world heating system.

Control logic tables for the heating system and auxiliary heater system are shown in Tables 1 and 2 respectively. The control logic ensures that defrosting is prioritized over other functions, the DHW tank is prioritized over space heating (SH), and that the total HP cycle length (on + off duration) cannot be <10 min. DHW tank temperature triggers tank heating if the tank mid node temperature falls below the lower hysteresis limit (49 °C by default) until the entire tank temperature exceeds the upper threshold (51 °C by default). The SH loop logic is identical, but tank temperature is replaced with reference zone temperature. An auxiliary direct electric heater is also incorporated on the DHW tank to boost tank temperature to 60 °C once a day (see 2.3.6 for full treatment of DHW).

Additionally, the heating system is activated/disabled by an input time series that prevents heating during times when the user does not require it (e.g. they are absent or asleep), and the hot water and space heating demand time series. The size of DHW tanks, thermostat hysteresis set points, and DHW set points are all adjustable.

The components of the heating system represented in the model introduced here can therefore be broken down into:

- A general hydronic circulation model
- ASHP/GSHP models
- Return side and flow side pipework models
- A bypass valve model
- Radiator node models (with integrated TRVs)
- An indirectly charged DHW tank model (with integrated heat exchanger and mixing valve)

The fundamentals of each of these components are described in greater detail in the following sub-sections.

2.3.2. General circulation model

The circulation model is a novel alternative to traditional pressure-flow based models, and determines the mass flow rate of water through each component in the circuit and allows calculation of the temperatures of radiator nodes. The governing equations for circulation pump flows are:

$$\begin{cases} \dot{m}_{circ} = \sum_{i=1}^{N_{rad}} \dot{m}_{rad} \quad \textit{where SH loop is active,} \\ \dot{m}_{circ} = \dot{m}_{limit} \quad \textit{where SH loop is active and } \sum_{i=1}^{N_{rad}} \dot{m}_{rad} < \dot{m}_{limit} \\ \textit{o} \\ \dot{m}_{circ} = 1.1 V_{DHWTank} \quad \textit{where DHW loop is active} \\ \textit{o} \\ \dot{m}_{circ} = 0 \quad \textit{where neither loop is active} \end{cases} \tag{7}$$

where $\dot{m}_{circ}$ is the total water flow rate through the circulation pump driving the system, and $\dot{m}_{limit}$ is the lowest flow rate required for ASHP/GSHP operation. Below this minimum level a bypass valve opens to ensure minimum flow is achieved. Bypass valve flow is calculated using:

$$\dot{m}_{bypass} = max\left(\dot{m}_{limit} - \sum_{i=1}^{N_{rad}} \dot{m}_{rad,n}, 0\right) X_{SH} \tag{8}$$

where X_{SH} value is 1 if the SH loop is active, and 0 otherwise. This ensures no flow occurs when the loop is registered as inactive. $\dot{m}_{rad,n}$ is the mass flow rate through radiator 'n', and is determined using Eq. (9)

$$\dot{m}_{rad} = \left[\frac{max(min((T_{set} - T_{room}) + 0.5\beta, \beta), 0)\dot{m}_{open}}{\beta}\right] X_{SH} \tag{9}$$

where $\dot{m}_{open}$ is the mass flow rate through the radiator when the TRV is fully open, β (in °C) represents the width of the valves linear region and the min and max functions ensure that the valve is fully open when $(T_{set} - T_{room}) > \frac{\beta}{2}$, and fully closed when $(T_{set} - T_{room}) < -\frac{\beta}{2}$. An example is that if $\beta = 4$, then TRV will be fully closed when the room is ≥ 2 °C warmer than the TRV set point (T_{set}). TRV will then fully open when the room is ≥ 2 °C cooler than the TRV set point, and TRV will progress linearly from open to closed across this range.

The circulation model presented in this study was based on the CARNOT blockset [16]. The blockset is capable of determining system pressure at any node on the thermohydraulic circuit, and in turn uses this to determine mass flow rates. However, this process is iterative and and takes more than 1000 times longer to compute than a system with predefined constant mass flow rates.

In reality, mass flow rates through radiators are not constant; a greater number of open TRVs results in higher mass flow and thus lower system pressures (Fig. 5) [27]. Multiple TRV openings cause lower system pressures and hence lower flow through any specific emitter when compared to when only one TRV is open. Therefore, mass flow through any given emitter is somewhat dependent on the state of the rest of the system, and defining mass flow rates as constant is incorrect.

A typical circulation pump (correctly sized) for the systems in question could deliver up to 40% lower pressure at full flow than at minimum flow [27]. A simple parallel pipe flow analysis with quadratic mass flow dependent pressure drop shows that there is less than 10% difference in flow rate between one radiator flow and full flow, and that this results in less than 1% difference in heat pump power demand, and little observable change in cycling behavior. Furthermore, against this complex backdrop, this work adapts the behaviour of modern circulation pumps which can operate at constant pressure or proportional pressure mode within a given range [27]. This novel approach reduces difficulties associated with the gap between theory and practice in pressure vs. flow dynamics, allows the model to perform at greater

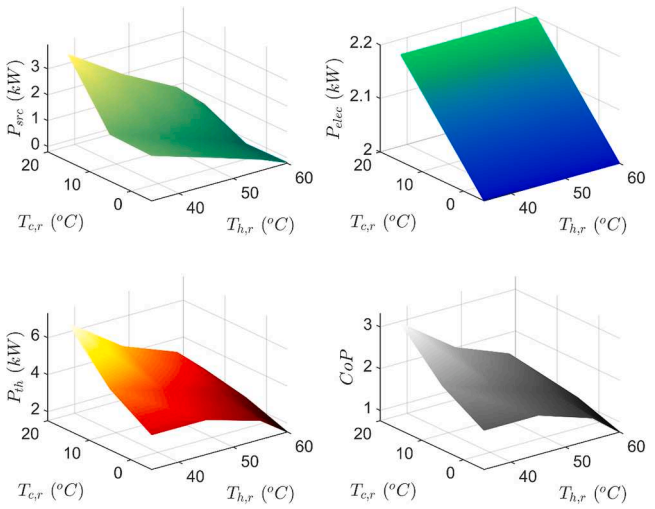

Fig. 6. Visualization of regression models for thermal input from source (top left), HP electrical power (top right), thermal supply to sink (bottom left) and pump coefficient of performance (bottom right).

computational efficiencies, and remains representative of proportionally controlled modern pumps within the space heating sub-model.

2.3.3. Radiator node

As mentioned in Section 2.2, the radiator energy balance is modelled using the '210' model detailed in [26]. Radiator nominal power, nominal temperature, and heat capacity are adjustable. However, EWASP is able to size radiators automatically based on standard methodology [28].

2.3.4. Secondary return node model

The secondary return (all pipework between the radiator outlets and heat pump) is modelled as one node, and is governed by the standard heat balance presented in Eq. (10):

$$m_{h,^\circ Ret} c_{Ret} \frac{\partial T_{h,^\circ Ret}}{\partial t} = \left[c_{H_2O} \left(\sum_{i=1}^{N_{rad}} (\dot{m}_{rad,n} T_{rad,n}) + \dot{m}_{bypass} T_{h,^\circ Flow} \right) \right] - \dot{m}_{HP} c_{H_2O} T_{h,^\circ Ret} \quad (10)$$

The right hand side terms denote the heat flow in and out of the secondary return pipework as a result of water flow. The expression $\dot{m}_{rad,n} T_{rad,n}$ ensures that the temperature, and flow rate of each radiator is taken into account when calculating the temperature change of the return pipework.

2.3.5. Heat pump & secondary flow node model

The ASHP and GSHP models are based on the heat pump blocks available from the CARNOT library [16], but novel modifications have been included that allow ramping and defrost to be considered. Input takes the form of matrices that define the heat output and electrical demand of the pump at different flow and source temperatures. The flow side of the heating system pipework is modelled as one node (similar to the return side represented in Section 2.3.4) and is represented using the standard heat balance presented in Eq. (11)

$$c_{h,^\circ Flow} \frac{\partial T_h}{\partial t} = \left[\dot{m}_{HP} c_{H_2O} \left(T_{h,^\circ Ret} - T_{h,^\circ Flow} \right) + \dot{Q}_{HP} \right] + U_{HP} A_{HP} \left(T_{out} - T_{h,^\circ Flow} \right) \quad (11)$$

where $T_{h,^\circ Ret}$ and $T_{h,^\circ Flow}$ are the return and flow temperatures respectively. The first right hand side term represents the change of stored heat in the flow side node as a result of inflow from the HP. The term $U_{HP} A_{HP} \left(T_{out} - T_{h,^\circ Flow} \right)$ represents conductive heat loss through the heat

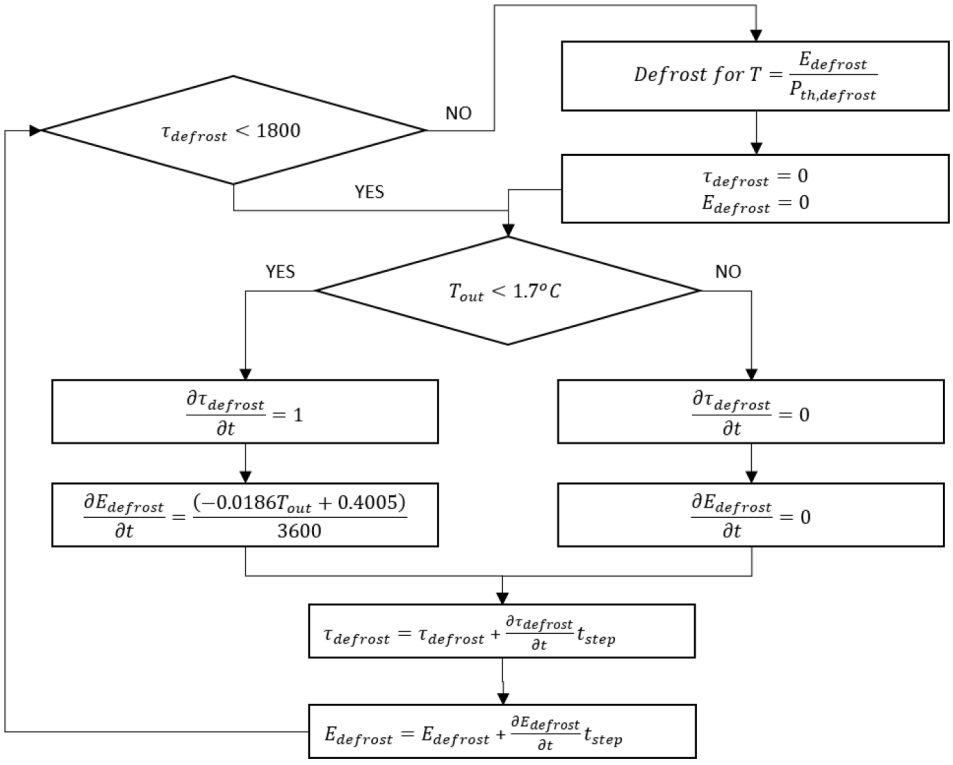

Fig. 7. Defrost logic schematic outlining the decisions and processes that govern defrost cycle start time and duration.

Table 3
Wind speed and direction and temperature gradient across building fabric for which building states are evaluated (leading to a total of 144 air flow patterns per building state).

Variable	Values
v_{wind}	0, 1, 2, 3, 5, 8, 12, 15, 18, 21, 25, 30
$\Delta T_{in\rightarrow out}$	0, 10, 20
Building face most directly in wind path	N, E, W, S

pump fabric. $\dot{Q}_{HP}$ is the heat gained via operation of the pump. In normal operation, it is represented with the CARNOT [16] regression model:

$$\dot{Q}_{HP} = K_1 T_{c,^\circ Ret} + K_2 T_{h,^\circ Flow} + K_3 \quad (12)$$

$T_{c,^\circ Ret}$ represents source temperature, which is the mean temperature of the ground boreholes in the GSHP case, and the ambient air temperature in the ASHP case. The K terms are fitting parameters for the regression model and are automatically determined from model input. When a building has been defined by the analyst, the setup framework in EWASP will automatically size to pump, such that it is large enough to maintain an indoor-outdoor temperature difference of 24.2 °C, which is in line with BRE recommendations [29].

The default case assumes if the heat pump has been running for fewer than 3 min, the heat gained by the water per second ramps linearly from 0 to $\dot{Q}_{HP}$ across this time period. This allows representation of the pump in non-steady state operation, which is important during very short runs. The 3-minute ramp reflects the findings of actual field studies [30,31]. It is possible for the user to change the ramping time for the pump during model initialization, as this time can vary between ASHP and GSHP models. The default regression model for a typical domestic heat pump is adapted from [16,31], and is visualized in Fig. 6.

The primary side is represented similarly in the GSHP case – differential equations represent cooling across the GSHP and heating through the ground source heat exchanger. A 10 node ground model is included to simulate the thermal dynamics of the ground condition surrounding the boreholes as suggested in [32].

The mass flow rate through the HP is approximated as the sum of flows through all radiators in the building plus that of the bypass valve.

The defrost logic outlined in [33] is used to approximate the requirement for and the duration of defrost cycles. At the beginning of the simulation, the second counter, $\tau_{defrost}$, is set equal to zero. For every second of operation below 1.7 °C, the counter is incremented by a value of 1, and the energy required to defrost the outdoor coil is increased by $\frac{\partial E_{defrost}}{\partial t} t_{step}$. When $\tau_{defrost} = 1800$ (30 mins), the pump defrosts for a time period equal to the energy required to defrost $E_{defrost}$, divided by the pumps' nominal defrosting thermal capacity, $P_{th,defrost}$. The heat required for defrosting is drawn from the hot loop, which in turn draws heat from the building or DHW tank. After defrosting, $\tau_{defrost}$ and $E_{defrost}$ are reset to zero, and the process restarts.

Fig. 7 summarises the defrost cycle logic.

The ASHP and GSHP models improve on more established building modeling platforms such as E+, which does not have detailed in-built heat pump modelling capabilities.

2.3.6. DHW

The DHW tank is modeled using a modified CARNOT DHW tank system with a single water to water heat exchanger (with typical effective U-values [34]), a mains inlet, an auxiliary element heater, and an outlet for DHW supply. Modifications were made to allow the model to run without computing Prandtl or Nusselt numbers (these were replaced with regression model approximations, which improved simulation rate by a factor of 3), and to add auxiliary heating capabilities. Whenever the central tank temperature ($T_{DHWTank}$) falls below a lower threshold, the indirect heating loop raises the temperature of the entire tank above an adjustable upper threshold. In order to mitigate legionella risk [35], once per day, the tank is brought to 60 °C by the auxiliary direct electric heater (the tank is set to reach a default maximum value of 51 °C by the heat pump). The immersion heater is automatically sized to ensure that the tank can be heated from water mains temperature to 60 °C within 2 h (1 kW per 60 l).

A thermostatic mixing valve is included at the DHW outlet to ensure a comfortable output temperature, and this is assigned probabilistically based on the DHW delivery temperature distribution taken from [36]. The flow mixer's behavior is determined using Eq. (13):

$$\dot{m}_{tank} = \frac{(T_{mains} - T_{DHW})}{(T_{mains} - T_{DHWtank})} \dot{m}_{DHW} \quad (13)$$

where the range of the term $\frac{(T_{mains} - T_{DHW})}{(T_{mains} - T_{DHWtank})}$ is between 0 and 1.

2.4. Airflow network model

Infiltration and ventilation airflows within UK homes are typically functions of stack and wind effects [28]. In its most complete form detailed knowledge of building fabric, opening characteristics, and microclimate are required for highly case specific treatment of infiltration and natural ventilation.

The EWASP model includes an air flow network model which uses approximate equivalent leakage area (ELA) inputs, and allows ventilation effects and temperature changes within zones to be approximated more realistically than in those models that use only ACR rates. Open internal doorways, Closed internal doorways, external surfaces, and stairwells are all considered.

Mass flow through building fabric is modelled using the equivalent leakage area (ELA) method from ASHRAE [28], which requires estimation of the ELA of each surface. ELA data for any given element at an indoor-outdoor pressure difference (ΔP_r) = $4Pa$ can be obtained from the ASHRAE handbook. Ideally, the ELA of each wall of each zone would be calculated in detail, but the time consuming nature of this approach and unrealistic quantities of input data required defeats the computationally effective purpose of the EWASP tool. It was found that determining a rough ELA for the whole building (i.e a value that gives the expected ACR at average wind speed and $\Delta T_{in\rightarrow out}$), then dividing the value amongst zones based only on their surface area provided similar results to a careful analysis of leakage area, and allowed very fast and simple configuration of the airflow network model. Therefore, room ELA values are estimated using the novel approximation Eq. (14)

$$ELA = h_z \times l_{w,ex} \times ACR_{nom} \times 6.54 \quad (14)$$

where h_z is the height of the zone, $l_{w,ex}$ is the external length of the wall for the associated zone and ACR_{nom} is the nominal air change rate of the building at average wind speeds and design temperature differences. Eq. (14) generates a set of ELAs from which ACR for any design conditions are derived.

The ASHRAE method requires that external pressures are defined. It is important to consider the external pressure experienced by a zone as a function of building shielding level, outdoor temperature, zone elevation, wind speed, and wind direction. By assuming the building is in some way shielded (the case for the overwhelming majority of UK residential buildings), the pressure on each face of the building can be approximated using Eq. (15), which is based on data from [37].

$$\begin{cases} P_{0,out} = \frac{1}{2}\rho(-0.25)v_{wind}{}^2, & wall\ not\ in\ direct\ wind\ path,\ ground\ floor \\ P_{0,out} = \frac{1}{2}\rho(0.2)v_{wind}{}^2, & wall\ in\ direct\ wind\ path, ground\ floor \\ P_{0,out} = \frac{1}{2}\rho(0.2)v_{wind}{}^2 - \rho_{out}(T)gh_{fl}, & wall\ in\ direct\ wind\ path, not\ ground\ floor \\ P_{0,out} = \frac{1}{2}\rho(-0.25)v_{wind}{}^2 - \rho_{out}(T)gh_{fl}, & wall\ not\ in\ direct\ wind\ path, not\ ground\ floor \end{cases} \quad (15)$$

where h_{fl} is the elevation above ground of the zone floor (only applicable for zones that are not on the ground floor).

Airflow through internal open/closed horizontal and vertical openings is modelled using the same opening and crack methods used by E+ [38].

The net airflow between zones, and from zones to the building exterior, under a given set of weather conditions, can be determined by finding the set of zone pressures that satisfy the following equation for each room:

$$\dot{m}_{n,out} + \sum_{m=1}^{n_{m,open}} \dot{m}_{nm,open} + \sum_{m=1}^{n_{m,closed}} \dot{m}_{nm,closed} + \dot{m}_{stairwell} = 0 \quad (16)$$

where $n_{m,open}$ and $n_{m,closed}$ are the number of adjacent room linked by open and closed door ways respectively. Though the airflow model can solve a single timestep in roughly 1 s, the airflow model increases the computational cost of running EWASP by a factor of 10^3 if a solution is determined for each timestep (at the default 5 s temporal resolution). Because usually only a small set of building states are considered (e.g. all doors open & all bedroom doors closed), pre-generation of air flow patterns for different weather states was chosen as an optimal point between high input data requirements and low computational cost. This is in contrast to commercial tool such as E+, that solve airflow during simulation.

With a small set of pre-generated input weather states, it is possible to generate hundreds of daily electrical demand profiles for a given house archetype per hour by varying occupancy, demand patterns, control settings, and technologies.

The weather conditions that building states are evaluated at are shown in Table 3. It is not necessary to evaluate airflow at all $\Delta T_{in\rightarrow out}$ values or all wind speeds (airflow results do not vary significantly with $\Delta T_{in\rightarrow out}$, or at wind speeds greater than ≈5 m/s, and linear interpolation is performed if airflow or $\Delta T_{in\rightarrow out}$ take between-state values). Wind direction is fixed to N, E, S, or W. When using this method, it is possible to evaluate one state for all weather conditions in about 60–70 s.

The net flow between zones was not greatly affected by normal inter-zone temperature variations or air turbulence, but bidirectional components of flow through an open doorway, and stairwell flow, were affected. Net airflow was broken into its components for the doorway and stairwell cases as outlined in [38]. This also means that bidirectionality algorithms need to be applied after the net airflow problems are solved. This is a further deviation from the airflow methods used in tools such as E+ that reduces computation cost without detrimental effects on results.

Table A1 (in Appendix section) outlines the limitations of the model, the mathematical reason for the limitations, and the future work to address these limitations.

Table 4
Required input data time series, the reasons for their inclusion, and where the default time series were obtained from.

Data	Purpose	Source
Direct Normal Irradiance	Used in determination of solar gains	Helioclim-3 satellite data [39]
Direct Irradiance angle (for N/E/S/W facing walls/windows	Used for determination of solar gains	Helioclim-3 satellite data [39]
Diffuse Irradiance	Used for determination of solar gains	Helioclim-3 satellite data [39]
Wind Speed	Used In airflow network model	Helioclim-3 satellite data [39]
Wind Angle	Used In airflow network model	Helioclim-3 satellite data [39]
Outdoor Temperature	Determine heat loss from conductive and infiltrative loss through the building fabric	MIDAS Open: UK Hourly Weather Observation Data [40]
Ground temperature	Determine losses through floor slab/temperature of ground in GSHP model	Derived from 'Soil surface temperatures reveal moderation of the urban heat island effect by trees and shrubs' [41]
Hot water Usage Profile	litre/min draw of hot water, used to determine change in stratified temperature profile of DHW tank	CREST synthesized (linked to an associated occupancy and electricity demand profile) [9]
Heating Active Profile	Used to determine whether any request for heating exists	CREST synthesized [9]. Assigned randomly from a profile pool via a monte-carlo process

Table 5
Modelled heat loss versus empirical average heat loss at $\Delta T_{in-out} = 24.2^oC$ in kW for a selection of archetypes with a given floor area. The empirical value is shown in brackets, and the range shows 'latest-earliest' data.

Heat Loss (kW)	Mid Terrace	End Terrace	Semi-detached	Detached
<1920	8.8 (8.1–9.1)	11.8 (11.0–14.8)	13.2 (12.0–15.5)	20.4 (17.6–22.1)
1950s	6.8 (6.8)	8.3 (8.7)	9.3 (9.2)	13.5 (14.7)
1980s	4.3 (4.6–4.9)	5.7 (5.4–6.2)	5.5 (5.3–6.4)	10.0 (9.5–10.1)
early 2000s	4.1 (4.0–4.7)	4.6 (4.5–5.8)	4.8 (4.2–5.1)	9.8 (9.1)

2.5. Input data requirements

Most of the time series and parameters required for the model to perform a simulation are already defined within archetypes that have been pre-programmed so that the analyst can approximate any building with only a knowledge of the building floorplan and age. In the following sections an overview of the time series data, archetypes, and requirements for archetype definition are given.

2.5.1. Time series data

Various time series of meteorological and social datasets are required to allow the model to run. These series, their purpose, and sources are summarized in Table 4. Mains inlet water is approximated as constant at 10 °C, as justified in [42].

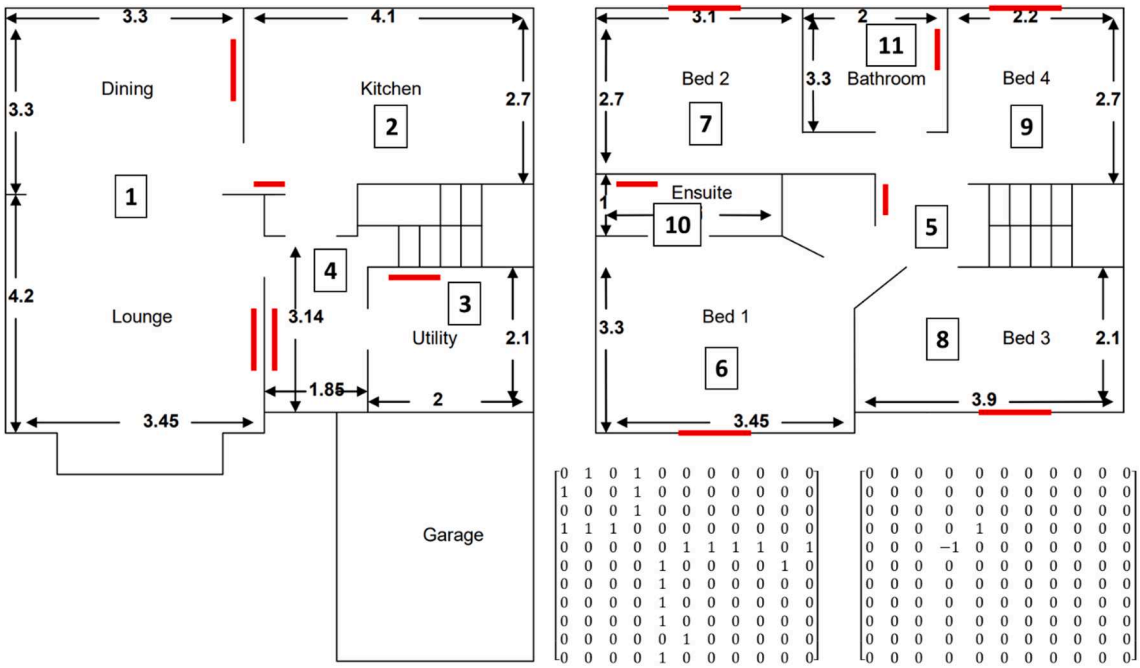

Fig. 8. The floorplan for the test house [30] and the associated horizontal and vertical convection matrices.

Table 6
Room dependent parameters used to represent the test house.

Property	Lounge/Dining	Kitchen	Util.	Hall	Land.	Bed 1	Bed 2	Bed 3	Bed 4	Bath.	En-suite
$A_{wall,1}$	8.28	0	0	4.44	0	8.28	14.20	9.36	0	0	0
$A_{wall,2}$	18.00	0	0	0	0	7.92	6.48	0	0	0	2.40
$A_{wall,3}$	7.92	9.84	0	0	0	0	7.44	0	5.28	4.80	0
$A_{wall,4}$	0	6.48	5.04	2.4	0	0	0	5.04	6.48	0	0
$A_{win,1}$	3.6	0	0	0	0	1.0	0	1.0	0	0	0
$A_{win,2}$	0	0	0	0	0	0	0	0	0	0	0
$A_{win,3}$	2.5	2.1	0	0	0	0	1.0	0	1.0	0	0
$A_{win,4}$	0	0	0	0	0	0	0	0	0	0	0
ACR_{nom}	0.7	0.7	0.7	0.7	0.7	0.7	0.7	0.7	0.7	1.5	1.5
$P_{th,nom}$	5200	547	1634	2400	700	2519	2519	2519	2519	1001	305
$\dot{m}_{rad}$	0.24	0.04	0.06	0.06	0.002	0.03	0.03	0.03	0.03	0.015	0.03
A_f	25.4	11.1	4.40	4.50	4.00	12.9	8.37	8.20	5.94	2.70	6.60

Table 7
Room independent parameters used to represent the test house.

Wall overall thickness (m)	0.27	RadiatorΔT_{nom}	40 °C
U_{wall} (W/m^{2}K)	0.30	Floor thickness (m)	0.20
c_{int} (brick) (kJ/m^2)	164.8	Floor type	Concrete Slab
c_{mid} (rockwool) (kJ/m^2)	5.25	ρ_{sl} (kg/m^3)	2350
c_{ext} (aerated concrete) (kJ/m^2)	65.0	c_{sl} (concrete, thickness 0.2 m) (kJ/m^2)	570
c_{win} (single 4 mm pane) (kJ/m^2)	8.0	$c_{furniture}$ (wood and plastic) (kJ/kg)	1.7
c_{roof} (kJ/m^2)	34.2	$c_{furniture}$ (soft furnishings) (kJ/kg)	1.4
U_{win} (W/m^{2}K)	2.10	Return flow hysteresis (°C)	37.5. 40
U_{rf} (W/m^{2}K)	0.15	Room Thermostat hysteresis (°C)	21.0 - 21.1 °C
U_{sl} (concrete, thickness 0.2 m) (W/m^{2}K)	0.50	$U_{intermed}$ (W/m^{2}K)	2.00
Target Radiator send-return ΔT (°C)	6. 7	Ceiling height (m)	2.3

2.5.2. *Predefined archetypes*

A set of archetypes have been pre-programmed to ensure ease of use. These represent UK Building Research Establishment (BRE) archetypes for a single family home (detached), a mid-terrace home, and an end-terrace home [43]. We also include semi-detached models, which use the same envelope properties as terraced houses (as per BRE recommendation). U-values are taken from the BRE database are based on building type and age. Fabric heat capacities, densities and dimensions for archetypes of different ages are based on advice for the University of the West of England [44], and chosen floorplans are based on typical layouts for the building type and age (by finding recurring layouts that closely match the suggested floor area [45]). For each archetype, It was ensured that heat loss properties reflect those measured empirically in [29] for the building type and age. The empirical and modelled steady state heat loss for a selection of the buildings at an indoor-outdoor ΔT of 24.2 °C are shown in Table 5. It should be noted that whilst building fabric properties are assigned in bands (i.e. houses build between 1920 and 1930 may be modelled with the same set of U values), these bands are not necessarily the same for all properties; for example, the same terraced house floor plan is used for all properties built between 1965 and 1989, but U values are assigned in the bands 1965–1980 and

Table 8
The system and control parameters, and a comparison of simulated (Sim) vs. Actual (Act) cycle results for a selection of control scenarios.

Pump	Control	TRV's open	T_{out}(°C)	L_{on} (min)		L_{total} (min)		$E_e\frac{sim}{act}$	$E_{th}\frac{sim}{act}$
				Sim	Act	Sim	Act		
ASHP	Hot Loop Return	All but 2 bedrooms	−5	37.2	38.1	40.3	42.4	0.97	0.96
		All open	5	12.0	11.2	18.5	17.8	1.07	1.07
		Lounge & dining open	7	5.3	6.6	15	16.2	0.91	1.00
		2 open	12	4.9	5.3	16	18.7	1.08	1.09
		All open	12	11.0	9.3	21	21.7	0.87	0.90
	Thermostat	Lounge & dining open	5	2.9	2.9	10.0	10.0	1.04	1.04
GSHP	Thermostat	Lounge & dining open	3.5	3.9	3.9	10.0	10.0	1.00	1.00
			7	2.4	2.6	10.0	10.0	1.06	1.08

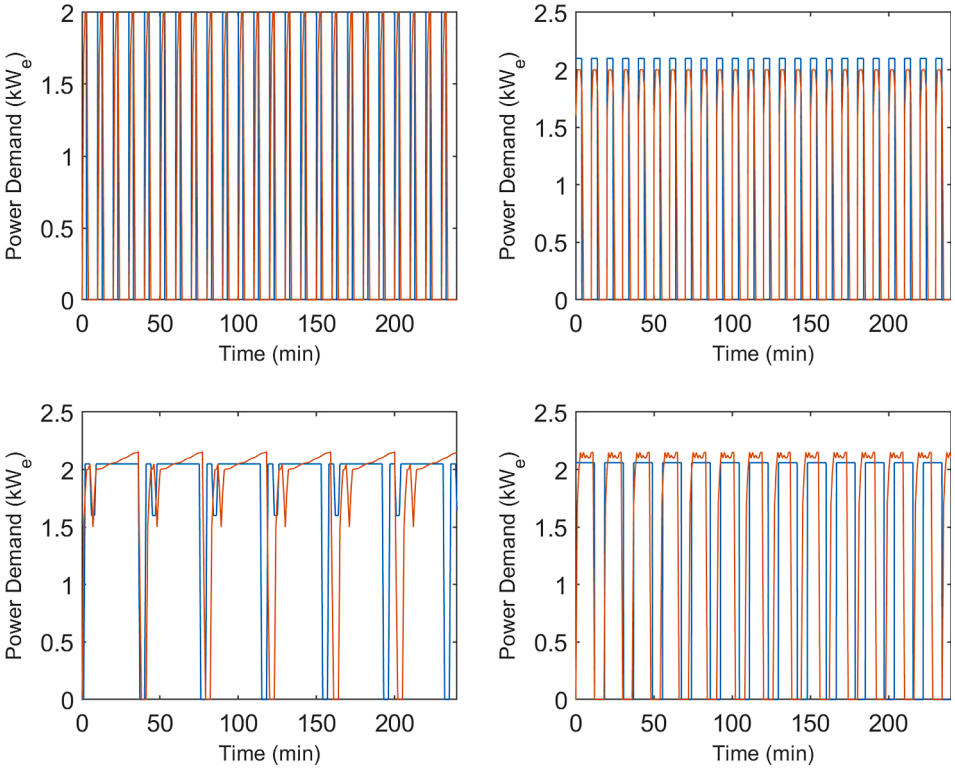

Fig. 9. The steady state modelled (blue) and real test house (orange) duty cycles for 4 scenarios: (i) top left: 5 °C ambient, ASHP, dining room and lounge TRVs open, controlled on room thermostat, (ii) top right: 3.5 °C ambient, GSHP, dining room and lounge TRVs open, controlled on room thermostat, (iii) bottom left: −5°C ambient, ASHP, 2 bedrooms' TRV's closed, controlled on hot loop temperature, (iv) bottom left: 5 °C ambient, ASHP, all TRV's open, controlled on hot loop temperature. (For interpretation of the references to colour in this figure legend, the reader is referred to the web version of this article.)

Table 9
RMSE, MAE, and MBE for the EWASP model when compared to real results across the 8 scenarios.

	RMSE	MAE	MBE
E_e (kWh)	0.06	0.05	−0.01
E_{th} (kWh)	0.16	0.12	0.02
L_{on} (min)	0.92	0.70	−0.03
L_{total} (min)	1.31	0.91	−0.74

1981–1990. This is necessary, as fabric properties evolved more quickly than layout and floor area during this period.

Radiator water volume is estimated directly from radiator nominal power output by assuming 1 L of water per 200 W of thermal power under nominal operating conditions [30]. Mass flow rate for each radiator can then be determined as follows:

$$\dot{m}_{rad} = \frac{\dot{Q}_{nom}}{\Delta T_{rad} C_{H_2O}} \quad (17)$$

Although radiator parameters are automatically generated, the EWASP model also allows manual adjustment of these parameters.

2.5.3. Definition of new archetypes

The EWASP model also offers the flexibility to define a new archetype without extensive understanding of the model structure. To allow this, a modifiable script has been constructed, which requires the user to define only a few simple parameters. These are building age and archetype, the horizontal and vertical zone connection pattern, the floor level each zone belongs to, zone floor and external wall area, zone window/door surface area (and their orientation), floor type and usage. This allows a full model parameterisation within 15 min, and partial parametrisation (when using a predefined layout) within 1 min. Instructions to users are available at [46].

3. Results

3.1. Validation of space heating component

It is essential to ensure that the cycling behaviour of the model represents actual air and ground sourced HPs. To investigate this, the EWASP model of a test house with known ASHP and GSHP cycling response (specifically the EA technologies test house shown in Fig. 8 [30]) was constructed. The test house is a 4 bedroom detached house built to mid-2000s standards, and has a design heat loss of 4.4 kW at

Table 10
Cycling and energy results for the single zone simulations case. Scenarios match those explored in the multi-zone case.

Pump	Control	TRV's open	T_{out} (°C)	L_{on} (min)		L_{total} (min)		$E_e\frac{mod}{act}$	$E_{th}\frac{mod}{act}$
				mod	act	mod	act		
ASHP	Hot Loop Return	All but 2 bedrooms	−5	Always on	38.1	Always on	42.4	1.11	1.10
		All open	5	30.4	11.2	40.0	17.8	1.22	1.24
		Lounge & dining open	7	5.5	6.6	15.3	16.2	1.11	1.07
		2 open	12	5.0	5.3	15.6	18.7	1.13	1.09
		All open	12	18.0	9.3	27.6	21.7	1.48	1.49
	Thermostat	Lounge & dining open	5	4.5	2.9	10.0	10.0	1.54	1.57
GSHP	Thermostat	Lounge & dining open	3.5	3.2	3.9	10.8	10.0	1.35	1.41
			7	3.3	2.6	10.0	10.0	1.27	1.27

Table 11
RMSE, MAE, and MBE for the single-zone model when compared to real results across the 8 scenarios.

	RMSE	MAE	MBE
E_e (kWh)	0.24	0.21	0.16
E_{th} (kWh)	0.73	0.59	0.46
L_{on} (min)	7.46	4.26	3.74
L_{total} (min)	8.28	4.48	2.90

−1 °C external and 21 °C internal temperature. Room level control logic (TRVs and thermostats), and building fabric parameters were taken directly from [30], and were used to configure the model (see Tables 6 and 7). These values resulted in an overall building heat loss characteristic equal to the 4.4 kW suggested in the EA documentation.

An important factor to consider during validation is whether the model is capable of producing cycles with similar properties to those observed empirically. We evaluate this by comparing the cycle lengths (on time during any cycle (L_{on}) and total cycle period length in minutes (L_{total})), electrical energy per hour (E_e), and heat energy per hour (E_{th}) of the modelled (sim) case and the test house (act) case. The majority of actual measurements were recorded in spring 2012, though the $T_{out} = -5^oC$ scenario was recorded in winter. The EWASP modelled house was permitted to reach thermal equilibrium conditions before measurements were taken, as to better match the conditions the test house was measured under. Once equilibrium was reached, cycling data was recorded for 4 h, again to match EA test house measurements. The results are presented in Table 8, and duty cycle comparisons for 4 scenarios are shown in Fig. 9. Absolute error statistics are shown in Table 9.

In absolute terms, the EWASP model predicted actual cycle lengths with high accuracy, as is evident from RMSE and MAE values for each of the four output metrics. In relative terms, the modelled overall heat demand/overall electrical demand was typically within 10% of actual demand, with just one result 13% lower than the actual electricity demand value (ASHP, return temp controlled, all open, 12 °C), however this translated to only 0.8 kWh per day under normal heating operation, which relative to the daily total electrical demand (SH + DHW) of 9–10 kWh is small. It should be noted that in the ASHP scenario at −5 °C, a defrost is regularly required. The predicted defrost cycle matched the real duration (see Fig. 9), and similar accuracy rates were achieved when comparing model output to observation at 0 °C. It should be noted that the exact cycle length is quite sensitive to outdoor temperature, to the extent that a temperature change of 0.2 °C, or a minor change to U-values can drastically alter the position of the defrost cycle within the cycle. However, the overall on–off duty cycle length and total energy consumption are markedly less sensitive to such changes.

Table 10 and 11 show the results of simplifying the model to a single zone equivalent (fabric nodes are still included). Whilst model accuracy is sometimes reasonable given the simulation order, it is much lower than in the multi-zone case. The reasons for this can be summarised as follows:

- In the room thermostat control scenarios, the single zone model assumes that all indoor space must be directly heated. In reality, the living zone is usually heated to temperature, whilst others stop heating at a lower temperature. Therefore, most rooms remain cooler than the one zone model suggests, and heat demand is over predicted.
- In the return temperature scenarios, the effective volume of heated space is much larger than a multi-zone model would consider. This is because radiators that would be closed off by TRVs in the multi-zone case (thus allowing the hot water loop to heat faster), cannot close, as there is no zone level control. Over prediction increases as more radiators are opened. This is because when few radiators are open, the water can be heated much faster than the radiators can distribute the heat. Conversely, if all radiators are open, heat is much more rapidly lost to the space.

The resulting energy consumption/heat provision varied from observations by up to 57%.

3.2. Validation of DHW component

Although the DHW tank model was based on a component from the CARNOT blockset, a novel simplified equivalent of this model was built and implemented. This component was modified to replace full calculation of Prandtl, Reynolds, and Nusselt numbers with regression approximations/general values. This was necessary to ensure a simulation rate high enough to allow large scale profile generation. This simplification did not cause a change in tank or system behaviour.

Comparison with tank charging results from [34] showed that

Table 12
Value in brackets represents projected speed of FFD model on i9-8950HK, based on ratio of single thread speeds (2545/1477 [47]).

Model	Processor	Isothermal Zones?	Scope	Control Sim.	Multi-zone	Solution rate (1 = real time)
FFD [14]	Intel Xeon E5-1603, 4-core CPU @ 2.8 GHz	No	Single Room	Yes	No	1.86. 2 (3.2–3.46)
CREST [9]	Intel i9-8950HK, 6- core CPU @ 2.9 GHz	Yes	House as single zone	No	No	28,800
EWASP	Intel i9-8950HK, 6- core CPU @ 2.9 GHz	Yes	Multi-zone house	Yes	Yes	5082 (state generation time not considered)

modelled charging times were within 2% of empirical observations.

3.3. Comparison of simulation speed

With model timestep set at 5 s and simulation period of 24 h, the model was typically able to complete a single simulation in 17 s. This is 5082X real time, and 1468X the predicted speed of a single room FFD simulation on the same processor. This does not include the time taken to generate the airflow patterns for different building states, but this only need be performed once per archetype, so contributes negligible time if the model is used for its intended purpose (to generate hundreds of profiles per archetype). A comparison of the speed of EWASP to FFD techniques and the CREST model is shown in table 12.

3.4. Cross platform comparison

To examine the behaviour of EWASP in comparison to conventional building modelling software, the test house was built in the E+ environment, and programmed with the same control criteria. A 5-day winter period was simulated to produce half hourly space heating electrical demand. 5 s EWASP results were aggregated to produce similar half hourly timesteps to enable a direct comparative analysis with E+ .

Cross platform results showed a strong correlation between EWASP and E+ predictions. Two minor differences were observed, first a slightly lower demand prediction from EWASP during day 1, and second a longer demand tail of E+ during day 4 (Fig. 10). The former is mostly attributable to differences in free gains schedules between the models, and in a small part attributable to minor differences in model initialization – the E+ model was allowed to reach true thermal equilibrium, whereas equilibrium was estimated for the EWASP model upon initialisation. The latter can be attributed to the differences in free gain simulations between the two models (appliance and occupant heat gains). Although the day 4 tail difference appears large on the graph, it actually only represents 1.1 kWh of electricity, about 1.9 kWh of heat. EWASP uses the free gains and occupant heat gains from CREST, whereas the E+ model uses standard appliance gain per unit area rules, and a usage schedule. Because appliance gains schedules do not match, there is a discrepancy of about 1.4 kWh of heat gain from appliances. Consequently, the test house in the EWASP model cools slower, and the ASHP never activates. It is important to note here that both models' internal gains profiles are entirely reasonable, as are the initial states of the buildings, but these unknowns will produce unavoidable differences between any physical building models.

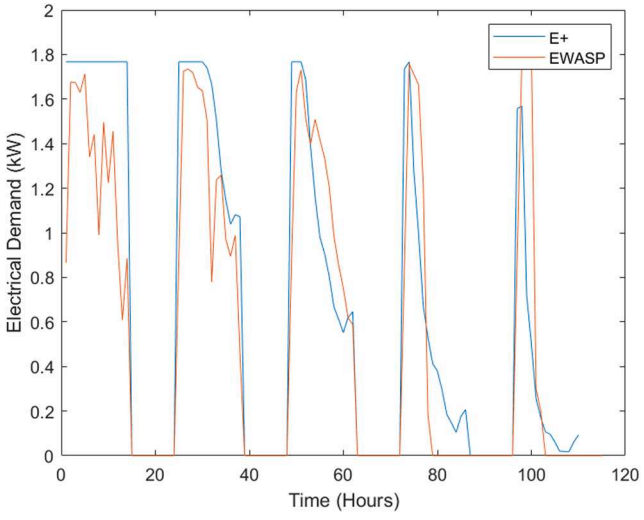

Fig. 10. Hourly EWASP and E+ electrical demand associated with space heating as a function of time across a 5-day wintertime period.

The latter results from EWASP's tendency to predict lower demand that E+ during thermostat setback periods. The sum of energy demand across the full time period is 6% lower in EWASP model.

The E+ model took nearly 40 h for a competent analyst to build and parametrise, compared to 15 min for the EWASP model. Whilst the E+ model was able to run 14 times faster than the EWASP model, it was due to 30-minute temporal resolution (DesignBuilder interface which assisted the geometry creation and was the interface used in this case and is limited to a minimum resolution of 30-minutes). Therefore, if both models were running at an equal temporal resolution, EWASP would be about 26x faster. The considerable time-saving offered by EWASP can enable extensive sensitivity, uncertainty and optimisation studies as a high fidelity model of heat pump duties reflecting any architypes can be created much more swiftly than comparative platforms.

4. Discussion and future work

Against empirical data and when compared to leading building energy platforms, the EWASP model presented in this work was shown to be capable of estimating the overall heat and electricity demands of residential buildings with ASHPs/GSHPs with good accuracy. In particular, EWASP is able to predict heat pump cycle properties to a notable degree of accuracy, especially considering the relatively low order of the simulation. The setup framework has been programmed such that it is able to construct an appropriate thermal model of a building of known layout and age with a relatively small pool of user input data, all of which could feasibly be obtained and applied in the model by an analyst without requiring advanced understanding of building physics and modelling, and the model has been shown capable of generating hundreds of daily profiles per hour, even when operating at 5 s resolution.

Though small differences between the EWASP and E+ results were noted, in magnitude and duration the load profiles were similar to the extent to suggest that the governing mathematics and their simplifications in EWASP model do not impact simulation results adversely. The comparison is not intended to suggest that one model is correct while the other is not, but to demonstrate how thermo-physical fabric properties, climate data and heated zones are interpreted by the two platforms when target temperatures are to be met by ASHP/GSHP. While EWASP model is open to the entire research community, in its current form it is intended to particularly aid studies in the following areas:

- The potential for provision of grid services via application of additional heating system control logic (e.g. provision of demand side response via dynamically changing thermostat bands).
- The potential for provision of grid services via combined control of multiple electrified loads (e.g. ASHP and EV).
- The effects of retrofit and control changes on high and low voltage network operation, as a function of network topology and building archetype mix.
- The effects of retrofit and control change on overall energy demand of residential buildings, to aid decision making in energy efficiency.
- The diversity factor of electrified heating loads as a function of building archetypes and the number of loads
- Ability to run buildings in batch control.

Whilst the model is currently suited to winter heating simulations, the project team intends to develop its capabilities in:

- Replacement of constant mains water temperature with time varying values, as the main water temperature experiences large seasonal variations.
- Improvement of the airflow model to allow open doors and windows to be considered, which will allow electrified cooling loads to be fully investigated. This will facilitate investigation of additional cooling loads under the effects of global warming, and applicability of the model to warmer climates.
- The addition of PV and solar thermal, for evaluation of the mitigation effect on demand these may bring about in both winter heating and summer cooling scenarios.
- Addition of further heating technologies, such as underfloor heating systems.
- Development of an addition set of predefined archetypes that represent net zero and active buildings.
- Modification of the model to accommodate forced ventilation systems; the model is not yet fully suitable for extremely airtight houses with mechanical ventilation. This is because the movement of air in such buildings is significantly different to that in a building with natural ventilation and higher infiltration rates. This development is likely to be a prerequisite to the creation of net zero and active building archetypes.
- Modification of the model to accommodate forced air heating systems; the model is not yet able to consider North American forced air type heating systems. However, hydronic heating is well represented in the model, which means it is of immediate use in Europe and Asia, where households with heating are almost exclusively fitted with hydronic systems.

5. Conclusion

The electrified water and space-heating model, a first-principle-based building energy simulation tool capable of rapidly generating thermal demand properties of a domestic building without the need for detailed input data or significant user expertise, has been outlined in this work. The model predicted actual cycle lengths to high accuracy, with modelled overall heat demand/overall electrical demand typically within 10% of actual empirical data. When benchmarked against a similarly parameterised EnergyPlus building and heat pump model, the model was able to produce heat pump demand profiles of similar magnitude and duration and displayed only 6% under-prediction of total energy demand against E+ when assessed across a full week of winter-time heating. The main advantage of the model is the simplicity of its parameterisation - without major accuracy penalties, a full model can be parameterised in around 15 min by an energy assessor using a fraction of parameter inputs required by other standard tools. This decreases parameterisation time by orders of magnitude when compared to advanced building energy simulation platforms such as EnergyPlus. The model is currently used to generate winter electrified heat demand profiles for the detailed analysis of heat pump control and fabric retrofit schemes, on local electrical networks. As such, the model is also applicable to energy efficiency analysis studies, where the energy efficiency differences arising from slightly different control and retrofit approaches are concerned. Future development of the model will focus on generation of heat pump cooling demand profiles, simulation of modern net zero/active buildings, and simulation of larger multi-family residential buildings (e.g. apartment blocks).

Funding

This work was supported by the EPSRC Active Building Centre (Grant Ref: EP/S016627/1).

CRediT authorship contribution statement

R.C. Johnson: Conceptualization, Data curation, Formal analysis, Investigation, Methodology, Validation, Resources, Visualization, Writing – original draft. **M. Royapoor:** Investigation, Methodology, Software, Resources, Validation. **M. Mayfield:** Funding acquisition, Supervision.

Declaration of Competing Interest

The authors declare that they have no known competing financial interests or personal relationships that could have appeared to influence the work reported in this paper.

Appendix A

The limitations of the models, and planned future developments, are shown in Table A1.

Table A1
Current limitations and planned future developments of the model.

Limitation	Logic	Future Developments
Not for heavily exposed buildings	Assumptions on the pressure variations around the building elements represent built-up urban zones	Expanding exposure level options to sub-urban and exposed rural sites
Not valid in instances in which ELA of a house is extremely non-uniform/summer scenarios in which doors and windows are open.	ELA is distributed based on zone external surface area and ACR.	Model will be modified to allow user definition of high leakage zones.

Appendix B

The three additional MATLAB interface consists of 3 inputs and 3 outputs. The 3 inputs are:

- Independent time series: time series input data that represents a parameter which is strongly decoupled from the heating system e.g. grid frequency, price signals.
- Building/heating system-dependent data: an output variable from the heating system model (e.g. the temperature of a particular room, tank temperature *etc.*) that is fed back into the interface.
- Control dependent Input: equal to control dependent output(s) at last timestep; represents the state of the interfacing system (e.g. electric vehicle (EV) state of charge, connection point voltage) as determined at the previous timestep.

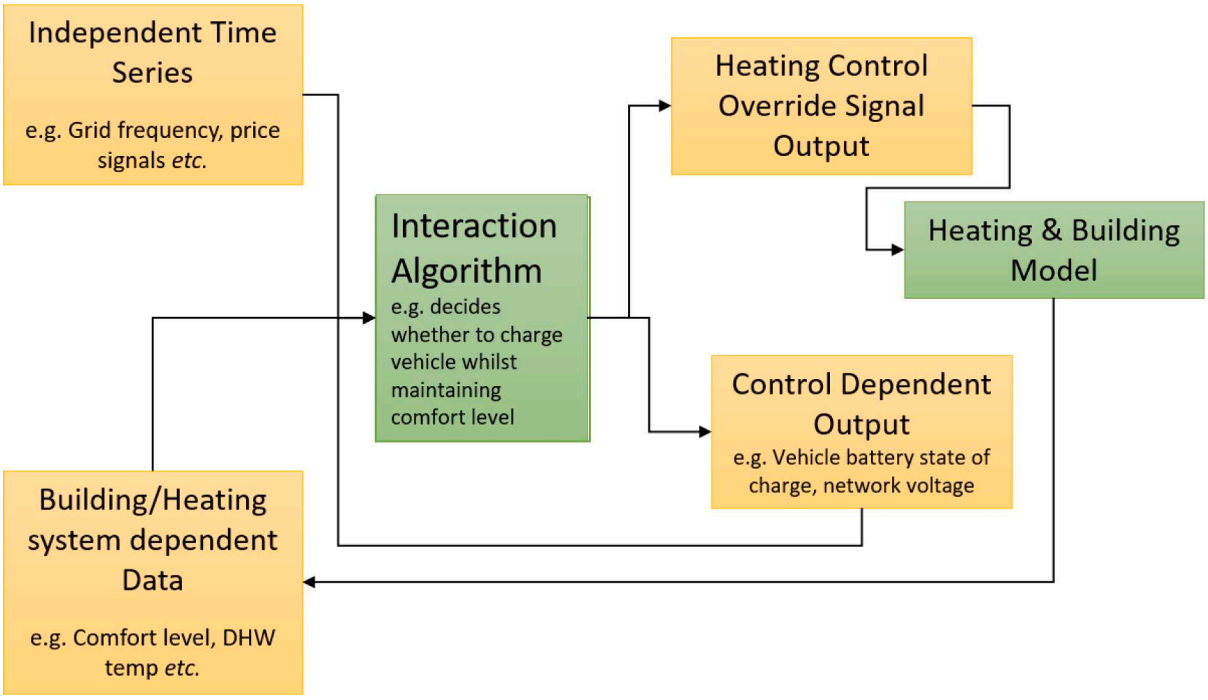

Fig. B1. The interaction between heating and building model, the interaction algorithm, and the interaction inputs and outputs.

The 3 outputs are:

- Control dependent output: represents the state of the interfacing system, determined by the changes implemented by the interaction algorithm.
- Heating control override signal: a binary output. If set to zero by the interaction algorithm, then the heating system switches off. If set to '1', the operation of the heating system will be governed by its standard operational logic.
- Setback control: a binary output. If set to 1, reduces the reference zone set point to 18 °C (the minimum recommended by Public Health England [48]).

Instructions on programming the interface are available at [46]. The overall interaction between inputs, outputs, the heating system model, and the interaction algorithm is shown in Fig. B1.

An example of interface utilisation, which concerns interaction between heating and an EV battery, is made available as supplementary material [46].

References

[1] IPCC. IPCC special report on the impacts of global warming of 1.5 °C. Geneva, Switzerland; 2018.
[2] Currie & Brown. A report for the Committee on Climate Change The costs and benefits of tighter standards for new buildings Final report. London, UK; 2019.
[3] Zidan A, Gabbar HA. DG mix and energy storage units for optimal planning of self-sufficient micro energy grids. Energies 2016;9(8):1–18.
[4] UK Power Networks. Impact of Electric Vehicle and Heat Pump Loads on Network Demand Profiles. London, UK; 2014.
[5] Navarro-Espinosa A, Mancarella P. Probabilistic modeling and assessment of the impact of electric heat pumps on low voltage distribution networks. Appl Energy 2014;127:249–66.
[6] Pimm AJ, Cockerill TT, Taylor PG. The potential for peak shaving on low voltage distribution networks using electricity storage. J Energy Storage 2018;16:231–42.
[7] Johnson RC, Mayfield M, Beck SBM. Utilization of stochastically located customer owned battery energy storage systems for violation management on UK LV residential feeders with varying renewables penetrations. 2018;19(June):52–66.
[8] bigladder software. EnergyPlus Manual; 2020. [Online]. Available: https://bigladdersoftware.com/epx/docs/ [accessed: 04-Feb-2020].
[9] McKenna E, Thomson M. High-resolution stochastic integrated thermal-electrical domestic demand model. Appl Energy 2016;165:445–61.
[10] Laughman CR, Mackey C, Bortoff SA, Qiao H. Modelling and Control of Radiant, Convective, and Ventilation Systems for Multizone Residences. Cambridge, Massachusetts; 2019.
[11] Hong J, Kelly NJ, Richardson I, Thomson M. Assessing heat pumps as flexible load. Proc Instit Mech Eng, Part A: J Power Energy 2013;227(1):30–42.
[12] Dogan T, Reinhart C. Shoeboxer: An algorithm for abstracted rapid multi-zone urban building energy model generation and simulation. Energy Build 2017;140:140–53.
[13] Wetter M. Multizone building model for thermal building simulation in modelica. Modelica conference 2006;2006:517–26.
[14] Jin M, Zuo W, Chen Q. Simulating natural ventilation in and around buildings by fast fluid dynamics. Numer Heat Transf Part A Appl 2013;64(4):273–89.
[15] Zuo W, Chen Q. Fast and informative flow simulations in a building by using fast fluid dynamics model on graphics processing unit. Build Environ 2010;45(3):747–57.
[16] Wohlfeil A. CARNOT Blockset. Germany: Remscheid; 2018.
[17] Feist Wolfgang. Thermische Gebäudesimulation - Kritische Prüfung unterschiedlicher Modellansätze. 1st ed. Heidelberg, Germany: Müller, Jur. Verl; 1994.
[18] Strobach E, Faiman D, Bader SJ, Hile SJ. Effective incidence angles of sky-diffuse and ground-reflected irradiance for various incidence angle modifier types. Sol Energy 2013;89:81–8.
[19] Feist W, Pfluger R, Hasper W. Durability of building fabric components and ventilation systems in passive houses. Energy Effic 2019;(Feist 1993).
[20] Kokogiannakis G, Darkwa J, Aloisio C. Simulating thermochromic and heat mirror glazing systems in hot and cold climates. Energy Procedia 2014;62:22–31.
[21] VirtualMaths. Conductivity of building Materials; 2018.
[22] Antalis. PERFORMANCE FLOORING Combilay- Ultra. Blaydon-on-Tyne, UK: Antalis; 2014.
[23] Carpet Institute of Australia. Thermal Insulation Performance of Carpet. Melbourne, Australia; 2002.
[24] Zhou J, Zhang G, Lin Y, Wang H. A new virtual sphere method for estimating the role of thermal mass in natural ventilated buildings. Energy Build 2011;43(1):75–81.
[25] Johra H, Heiselberg P. Influence of internal thermal mass on the indoor thermal dynamics and integration of phase change materials in furniture for building energy storage: A review. Renew Sustain Energy Rev 2017;69(May 2016):19–32.
[26] Hensen JLM. On the thermal interaction of building structure and heating and ventilation system - (Dissertation). Technische Universiteit Eindhoven Netherlands; 1991.
[27] Grundfos. ALPHA2 L Circulator pumps. Bjerringbro, Denmark: Grundfos.
[28] ASHRAE. ASHRAE Handbook 2001 Fundamentals; 2001.
[29] BRE. Dwelling Heat Losses; 2018. [Online]. Available: https://www.bre.co.uk/heatpumpefficiency/dwelling-heat-loss [accessed: 10-Jul-2018].
[30] Green R, Knowles T. The effect of Thermostatic Radiator Valves on heat pump performance. 2011;(June):21.
[31] Green R. The Effects of Cycling on Heat Pump Performance. 2012;(November):53.
[32] Albers K-J. Untersuchungen zur Auslegung von Erdwärmetauschern für die Konditionierung der Zuluft für Wohngebäude, Forschungsberichte des Deutschen Kälte- und Klimatechnischen Vereins. Hannover, Germany.

[33] Wu W, Skye HM, Domanski PA. Selecting HVAC systems to achieve comfortable and cost-effective residential net-zero energy buildings. Appl Energy 2018;212:577–91.
[34] Goonesekera AK. Performance Optimisation of Hot Water Cylinders. University of Sheffield 2017.
[35] Lévesque B, Lavoie M, Joly J. Residential water heater temperature. Can J Infect Dis 2004;15(1):11–2.
[36] Energy Saving Trust. Measurement of Domestic Hot Water Consumption in Dwellings. London, UK; 2008.
[37] Orme M, Liddament M, Wilson A. Numerical Data for Air Infiltration & Natural Ventilation Calculations. Warwick, UK; 1998.
[38] Bigladder software. Airflow Network Model; 2020. [Online]. Available: https://bigladdersoftware.com/epx/docs/8-3/engineering-reference/airflownetwork-model.html#airflownetwork-model [accessed: 24-Feb-2020].
[39] SoDa. Helioclim-3 Satellite data; 2005.
[40] Office M. Met Office Integrated Data Archive System (MIDAS) Land and Marine Surface Stations Data (1853-current). NCAS British Atmospheric Data Centre; 2016. date of citation.
[41] Edmondson JL, Stott I, Davies ZG, Gaston KJ, Leake JR. Soil surface temperatures reveal moderation of the urban heat island effect by trees and shrubs. Sci Rep 2016;6:1–8.
[42] Paurine A, Maidment G, Ford A. The potential use of the mains water loop for cooling, heat and energy networks. Cibse 2015;no. October.
[43] TABULA EPISCOPE. Building Typology Brochure England September 2014. Watford, UK; 2014.
[44] University of the West of England. Evolution of Building Elements; 2019. [Online]. Available: https://fet.uwe.ac.uk/conweb/house_ages/elements/print.htm [accessed: 29-Oct-2019].
[45] EHS. Floor Space in English Homes - main report. London, UK; 2017.
[46] Johnson RC. EWASP_v1.2; 2021. [Online]. Available: https://data.mendeley.com/datasets/82sck9pckz/1.
[47] PassMark Software. CPU Performance Comparison; 2019. [Online]. Available: https://www.cpubenchmark.net/compare/Intel-i9-8950HK-vs-Intel-Xeon-E5-1603/3246vs1209 [accessed: 05-Nov-2019].
[48] v1. https://publichealthmatters.blog.gov.uk/2014/10/21/preventing-avoidable-deaths-this-winter/; 2014. [accessed 22-Jan-2021].